Magnetic Resonance Imaging of Coronary Arteries

17

Mehmet Akçakaya and Reza Nezafat

Abstract

Coronary artery disease remains the leading cause of death in the United States, despite significant efforts in prevention and treatment. Coronary artery magnetic resonance imaging is a non-invasive diagnosis technique among patients with suspected anomalous coronary artery disease and coronary artery aneurysms. In this chapter, we will review the imaging strategies for magnetic resonance imaging of coronary arteries and veins. We review techniques for compensating the near-constant motion of the coronaries during both the respiratory and the cardiac cycles, for improving signal-to-noise ratio and contrast-to-noise ratio, advanced methods for accelerated imaging and high-field imaging, and coronary vein imaging.

Keywords

Coronary artery disease • Coronary magnetic resonance imaging • Respiratory motion • Cardiac motion • Motion compensation • Accelerated imaging • High-field imaging • Coronary vein imaging • T_1 contrast • T_2 contrast

Introduction

Coronary artery disease (CAD) remains the leading cause of death in the United States, accounting for one of every six deaths, despite significant efforts in prevention and treatment [1]. Each year approximately 635,000 Americans are estimated to have a new myocardial infarction, and nearly 280,000 to have a recurrent infarction. Furthermore, an additional estimated 150,000 will have their first silent myocardial infarction [1]. The current clinical "gold standard" for the diagnosis of significant (≥50 % diameter stenosis) CAD is catheter-based invasive x-ray angiography. More than a million catheter based x-ray coronary angiograms are performed annually in the United States [1], with a higher volume in Europe. However, a recent study of nearly 400,000 patients referred for x-ray coronary angiography showed that only less than 40 % had obstructive CAD, a relatively low yield for an invasive test [2]. Many of these patients without significant CAD were exposed to the potential risks and complications of an invasive test that includes ionizing radiation and iodinated contrast [3, 4]. Furthermore, selected high risk populations such as those patients with aortic valve stenosis, the incidence of subclinical stroke associated with retrograde catheter crossing of the stenotic valve may exceed 20 % [5]. In order to relieve symptoms, percutaneous coronary intervention in single vessel disease is commonly performed, but the greatest impact on mortality occurs with mechanical intervention among patients with left main (LM) and multivessel CAD. Thus, alternative non-invasive imaging modalities, which allow direct visualization of the proximal/mid native coronary vessels for the accurate identification/exclusion of LM/multivessel CAD, are desirable.

Coronary artery magnetic resonance imaging (MRI) has evolved as a non-invasive diagnosis alternative to

M. Akçakaya, PhD • R. Nezafat, PhD (✉)
Department of Medicine, Beth Israel Deaconess Medical Center, Harvard Medical School, Boston, MA, USA
e-mail: rnezafat@bidmc.harvard.edu

M.A. Syed et al. (eds.), *Basic Principles of Cardiovascular MRI: Physics and Imaging Technique*,
DOI 10.1007/978-3-319-22141-0_17

catheter based x-ray angiography among patients with suspected anomalous coronary artery disease and coronary artery aneurysms. Over the past two decades, it has reached sufficient maturity to obviate the need for catheter based x-ray angiography in the discrimination of patients with multivessel disease. Though, coronary multi-detector computed tomography (MDCT) offers superior isotropic spatial resolution and more rapid imaging, coronary MRI, is advantageous to MDCT in several respects, including the absence of ionizing radiation or iodinated contrast, which facilitates follow-up scanning, as well as smaller artifacts related to epicardial calcium. Due to the advantages of coronary MRI and its diagnostic accuracy, it is recommended and deemed appropriate in patients suspected of anomalous coronary artery disease by both the American College of Cardiology and American Heart Association [6, 7]. In this chapter, we will review the imaging strategies for magnetic resonance imaging of coronary arteries and veins.

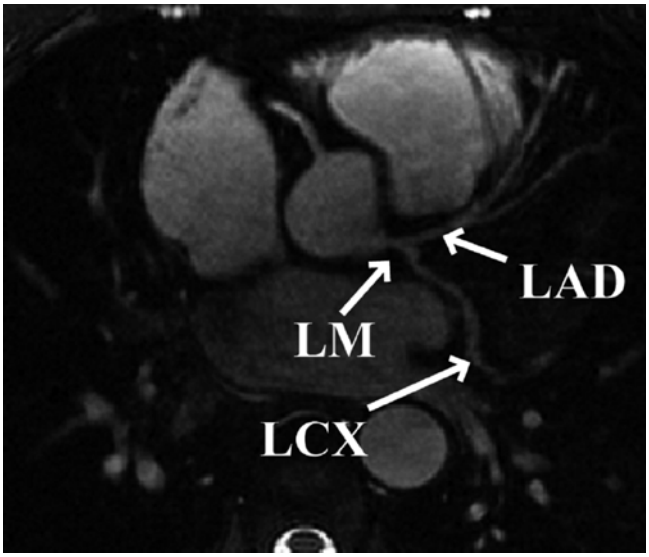

Fig. 17.1 Reformatted coronary MRI of the left coronary system acquired using a targeted free breathing acquisition with real time navigator gating and tracking in a healthy adult subject. The transverse acquisition displays the left main (*LM*), left anterior descending (*LAD*) and the left circumflex (*LCX*) coronary arteries. The in-plane spatial resolution is 0.7×1.0 mm^2

Coronary Artery MRI

Imaging Sequences

The early approaches to coronary MRI have been based on 2D breath-hold electrocardiogram (ECG) triggered segmented sequences, described nearly two decades ago [8, 9]. Over the past two decades, 3D free-breathing approaches have replaced these sequences, since they enable greater anatomical coverage and higher signal level. Either targeted or whole-heart coverage of the coronary anatomy is possible in 3D coronary MRI. In the targeted technique [10], a double-oblique 3D volume aligned along the major axis of the left or right coronary artery is acquired [11–13]. For the visualization of the left main (LM), left anterior descending (LAD) and left circumflex (LCX) coronary arteries, a 3D volume is interactively prescribed in the axial plane centered about the LM coronary artery, typically with a 30-mm slab with 20 overlapping using a segmented acquisition (Fig. 17.1) [13, 14]. For imaging of the RCA, the imaging plane passing through the proximal, mid and distal coordinates of the RCA is identified and the targeted 3D coronary sequence is repeated in this orientation. In whole-heart coronary MRI [15–29], in a manner analogous to coronary MDCT, an axial (or coronal) 3D volume encompassing the entire heart is sampled in a single acquisition. This facilitates imaging slab prescription and provides more complete anatomical coverage, positioned ~1 cm above the LM and extending to the inferior cardiac border. However, based on single-center trials up to date, it has not been shown to be superior to the targeted approach for CAD assessment (Table 17.1).

Both gradient echo (GRE) and steady state free precession (SSFP) sequences [38] have been used for targeted thin-slab 3D acquisitions. Thin-slab 3D targeted acquisition with a GRE sequence results in more homogenous blood pool signal, but is heavily dependent on the inflow of unsaturated protons [39]. If coronary flow is slow or stagnant, saturation effects will cause a local signal loss that is often relatively exaggerated as compared with the lumen stenosis. Compared to GRE sequences, SSFP provides intrinsically higher signal due to its balanced gradients and improved blood-myocardium contrast due to its T_1/T_2 weighting [40] with reduced sensitivity to inflow effects. Both GRE and SSFP have been used for targeted 3D coronary MRI, where both have shown similar diagnostic accuracy for CAD [40, 41]. For whole-heart non-contrast coronary MRI at 1.5 T, SSFP appears to be the sequence of choice due to its higher blood-myocardium contrast and superior inflow properties [39].

Even with these technical advances, clinical acceptance of coronary MRI remains challenging due to coronary artery motion, long scan times, limited spatial resolution, suboptimal signal-to-noise-ratio (SNR) and blood-myocardium contrast-to-noise-ratio (CNR). The technical challenges in coronary artery MRI is different than other cardiovascular magnetic resonance (CMR) acquisitions due to unique issues including: (1) small caliber of coronary arteries (3–6 mm diameter), (2) high level of tortuosity, (3) near-constant motion during both the respiratory and the cardiac cycles, and (4) surrounding signal from adjacent epicardial fat and myocardium.

Table 17.1 Diagnostic accuracy of ECG-triggered, free-breathing, targeted 3D and whole-heart coronary MRI with and without contrast agents

Study	Single-center/multi-center	# patients	Sensitivity (%)	Specificity (%)
Non-contrast 3D targeted coronary MRI				
Kim et al. [10]	Multi-center	109	88–98	32–52
Bunce et al. [30]	Single-center	46	50–89	72–100
Sommer et al. [31]	Single-center	107	74–88	63–91
Bogaert et al. [32]	Single-center	21	85–92	50–83
Non-contrast 3D whole-heart coronary MRI				
Jahnke et al. [33]	Single-center	21	79	91
Sakuma et al. [27]	Single-center	39	82	91
Sakuma et al. [26]	Single-center	131	82	90
Pouleur et al. [34]	Single-center	77	100	72
Kato et al. [35]	Multi-center	138	88	72
Contrast enhanced 3D whole-heart coronary MRI				
Yang et al. [36]	Single-center	62	94	82
Yang et al. [37]	Multi-center	272	91	80

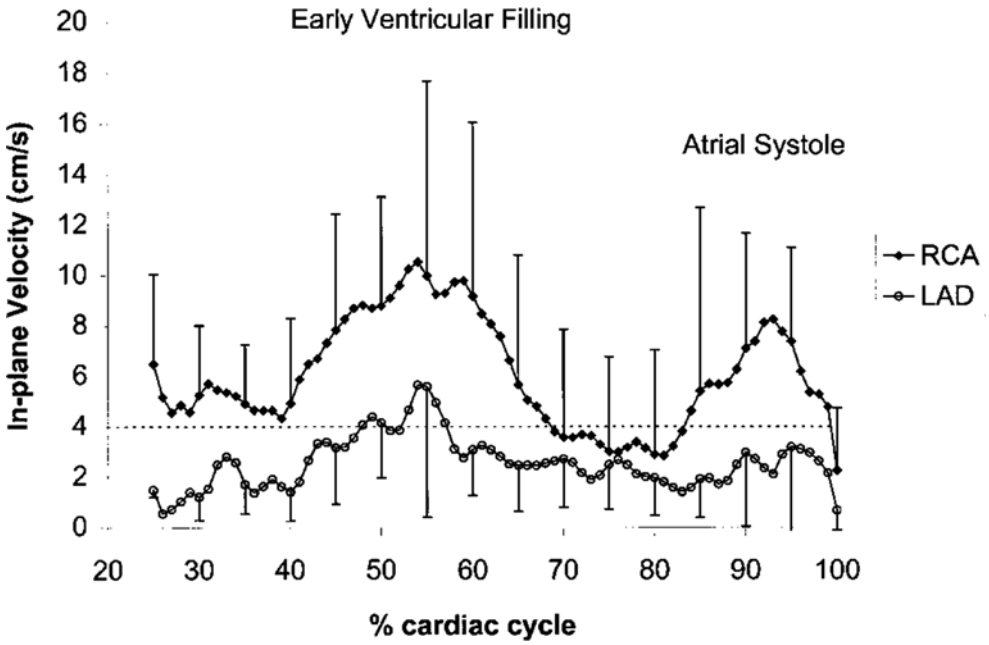

Fig. 17.2 Graph depicting the in-plane motion of the right coronary artery (*RCA*) and the left anterior descending (*LAD*) coronary artery during the cardiac cycle. The x-axis displays time as a percentage of the R-R interval. Note the image quality of the RCA cross section improves when the acquisition is performed during mid-diastole as compared to early diastole (Reproduced from [47], with permission of Wiley)

Cardiac Motion

Bulk epicardial motion is a major impediment to coronary artery and vein MRI and can be separated into motion related to direct cardiac contraction/relaxation during the cardiac cycle and that due to superimposed diaphragmatic and chest wall motion from respiration. The magnitude of motion from each component may greatly exceed the coronary artery diameter, thereby leading to blurring artifacts in the absence of motion-suppressive methods.

To compensate for bulk cardiac motion, accurate electrocardiographic (ECG) synchronization with QRS detection is required, and vector ECG approaches are preferred [42]. Coronary motion has been characterized using both catheter based x-ray angiography [43, 44] and CMR [45–47] methods during the cardiac cycle. Both the proximal/mid right coronary artery (RCA) and the left anterior descending (LAD) coronary artery display a triphasic pattern (Fig. 17.2), with the magnitude of in-plane motion nearly twice as great for the RCA. Coronary motion is minimal during isovolumic relaxation, approximately 350–400 ms after the R wave, and again at mid-diastole (immediately prior to atrial systole). The LAD diastasis is longer than the RCA, and begins earlier in the cardiac cycle [12]. The duration of the mid-diastolic diastasis period is inversely related to the heart rate and dictates the coronary data acquisition interval.

For coronary artery MRI, the acquisition interval is adapted to the heart rate/diastasis interval using a patient-specific diastasis period. This can be readily identified by the acquisition of high temporal resolution cine dataset orthogonal to the long axis of the proximal/mid RCA and of the LAD. Semi-automated tools to identify the optimal data acquisition window have also been proposed [48, 49]. For patients with a heart rate of 60–70/min, a coronary artery MRI acquisition duration of ~80 ms during each cardiac cycle results in improved image quality [14]. The duration must be further abbreviated (e.g., <50 ms) at higher heart rates, while with bradycardia, the acquisition interval can be expanded to 120 ms or longer. The use of patient-specific acquisition windows serves to reduce overall scan time [50, 51]. Image degradation can be caused by sinus arrhythmia, leading to heart rate variability, which is common especially in younger adults [52]. An adaptive real-time arrhythmia rejection algorithm can correct for heart rate variability, and improves coronary artery MRI quality [49].

Respiratory Motion

The second major challenge for coronary artery MRI is compensation for respiratory motion. With inspiration, the diaphragm may descend up to 30 mm and the chest wall expands – resulting in an inferior displacement and anterior rotation of the heart [53]. Several approaches have been proposed to minimize respiratory motion artifacts, including sustained end-expiratory breath-holding, chest wall bellows, respiratory navigators, fat navigators and self-gating methods.

Prolonged (15–20 s) end-expiratory breath holds were utilized to suppress respiratory motion in initial 2D coronary artery MRI methods [54]. Breath holding offers the advantage of relative ease of implementation in compliant subjects, but it limits the temporal acquisition window, image spatial resolution and anatomic coverage. Additionally, many patients are unable to adequately sustain a breath-hold. Furthermore, slice registration errors (due to variability in end-expiratory diaphragmatic position) are very common as is diaphragmatic drift during the breath hold [54–57] and may occur in up to half of patients [12]. Supplemental oxygen and hyperventilation (separately or in combination) can be utilized to prolong the breath-hold duration [56, 57], but these methods may not be appropriate for all patients, and both diaphragmatic drift and slice registration errors persist [57].

Diaphragmatic respiratory navigators, first proposed by Ehman [58] for abdominal MR imaging, enable free-breathing acquisitions without the stringent time constraints and patient cooperation requirements imposed by multiple breath holds, and thus offer superior spatial resolution opportunities. Although the specifics of navigator implementation varies among CMR vendors, in the ideal implementation, the navigator can be positioned at any interface that accurately reflects respiratory motion, including the dome of the right hemidiaphragm (Fig. 17.3) [59, 60], the left hemidiaphragm, the anterior chest wall, the anterior free wall of the left ventricle [60, 61], or even through the coronary artery of interest. The navigator should not cause an image artifact and should be temporally located *immediately* preceding the imaging portion of the sequence with data accepted (used for image reconstruction) only when the navigator indicates that the "interface" (e.g., diaphragm position) falls within a user-defined window. The dome of the right hemidiaphragm has become the preferred location [27, 38–40] due to the simplicity and ease in set-up, where the motion of the right hemidiaphgragm in the superior-inferior direction can be tracked. From CMR studies of cardiac border position during the respiratory cycle, Wang observed that at end-expiration, the ratio between cardiac and diaphragmatic displacement is ~0.6 for the RCA and ~0.7 for the left coronary artery [53] though there is variability among subjects [20, 42, 43] and position (e.g., supine vs. prone imaging) [23]. This rule-of-thumb offers the opportunity for prospective navigator gating with real-time tracking [60, 62], in which the position of the interface (diaphragm) is determined, and the slice position coordinates can then be shifted in real-time (before the data collection) to appropriately adjust spatial coordinates [63]. This technique allows for the use of wider gating windows and increased navigator efficiency, leading to shorter scan times. Real-time tracking implementation with a 5-mm diaphragmatic gating window is often used resulting in a navigator efficiency approaching 50 % [62]. Coronary artery MRI with real-time navigator tracking has been shown to minimize registration errors (as compared with breath holding) while maintaining or improving the image quality [12, 62]. It should also be noted that the quality of coronary artery MRI is improved by using consistent ECG timing as well as respiratory suppression methodology for both the coronary localizing/motion scout images and for the coronary artery MRI acquisitions [51].

A number of refinements to the navigator method have been proposed. While a "fixed" superior-inferior correction factor of 0.6 (with no left-right or anterior-posterior correction) [44, 45] is commonly used, significant individual variability has been observed [55]. A subject-specific tracking factor has been advocated and shown to improve the quality of coronary images when the subject-specific tracking factor differs from 0.6 [64]. The use of multiple navigator locations, use of leading and trailing navigators, and navigators that provide guidance for affine transformations, i.e. 3D translations and rotations, of the slice prescription for each heart-beat have been proposed [23, 65–67]. The affine transformation permits use of larger navigator windows, and hence higher navigator efficiency. It has also been proposed that the heart itself be tracked [20, 68–70]. For instance, methods that track the epicardial fat to detect the heart position have been proposed

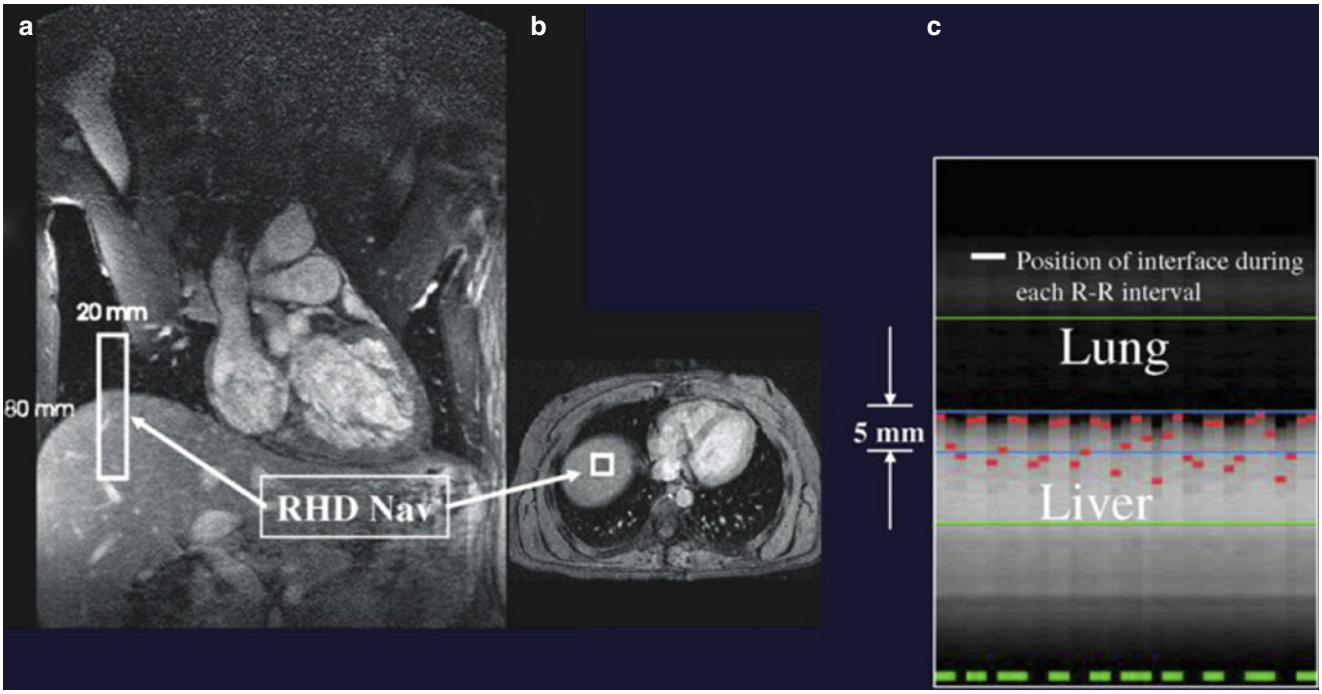

Fig. 17.3 Positioning and utility of the respiratory navigator. Coronal (**a**) and axial (**b**) thoracic images for placing the navigator at the dome of the right hemidiaphragm (RHD NAV). (**c**) Respiratory motion of the lung-diaphragm interface is recorded using a 2-D selective navigator with the lung (superior) and liver (inferior) interface. In this example, the maximum excursion between end-inspiration and end-expiration is ~11 mm. The position of the lung-liver interface at each R-R interval is indicated by the *broken line* in the middle of (**c**). Data are only accepted if the lung-liver interface is within the acceptance window of 5 mm. Data acquired with the navigator outside of the window are rejected. Accepted data is indicated by the *broken green line* at the bottom of (**c**)

[71–74]. In addition to navigator gating, respiratory self-gating techniques have been investigated, a method that derive the respiratory position of the heart from the imaging data itself [19, 20, 28, 68, 69, 75, 76], thus avoiding certain issues with navigators such as subject-dependent tracking factor [77] and hysteresis effects [78]. Navigator with fixed scan efficiency has also been recently introduced which results in imaging at a fixed scan time [79]. Novel k-space trajectories and various image reconstruction based method such as cross-correlation of low resolution images have also been proposed for respiratory motion compensation [28, 80–82].

SNR and CNR

The coronary arteries are surrounded by epicardial fat and the myocardium. Thus contrast-to-noise ratio (CNR) can be improved by suppressing the fat and myocardium signal surrounding the coronary arteries. Frequency (spectrally) selective pre-pulses are applied to saturate signal from fat tissue, thereby allowing visualization of the underlying coronary arteries [54, 83]. To differentiate myocardium and the coronary lumen, endogenous contrast preparation techniques are commonly utilized [14, 83–86]. Two methods that can enhance the contrast between the coronary lumen and underlying myocardium are T_2 preparation pre-pulses [14, 84, 85, 87] and magnetization transfer contrast [83, 86]. The former is often used for coronary artery MRI as it also suppresses deoxygenated venous blood, while the latter is used for coronary *vein* MRI [57].

The limited signal-to-noise ratio (SNR) in coronary artery MRI, along with constraints on acquisition duration, restricts the spatial resolution in the acquisition. Spatial resolution requirements for clinical coronary artery MRI depend on whether the goal is to identify the origin and proximal course of the coronary artery (e.g., issues of anomalous coronary disease), or whether the goal is to identify focal stenoses in the proximal and middle segments.

The SNR of coronary MRI can be enhanced by higher B_0 field strength [88], larger 3D spatial coverage [29], vasodilator administration, and contrast agents based on gadolinium chelates. The intrinsically higher SNR associated with higher magnetic field strengths may be advantageous for non-contrast coronary MRI. However, additional considerations, such as higher B_1 and B_0 inhomogeneity and higher specific absorption rate, affect certain aspects of coronary MRI, such as the diminished utility of SSFP sequences at 3 T due to increased field inhomogeneity and high specific absorption rate. Hence, GRE sequences, which are less sensitive to field inhomogeneity, as well as localized shimming [89] and

contrast preparation techniques that deal with B_1 inhomogeneities [87, 90] have been advocated.

The increased coverage of whole-heart coronary MRI can potentially improve the SNR but this also increases the scan time. Thus, the SNR gain is often counteracted by the need for accelerated imaging to reduce scan time, which carries an SNR penalty. Despite this penalty, excellent image quality of whole-heart coronary MRI has been shown in several studies [26, 29], and an example from a single-center study [26] is depicted in Fig. 17.4. Furthermore, whole-heart imaging suffers from saturation effects of the inflowing blood magnetization [39]. Another technique to improve SNR in coronary MRI is the administration of vasodilators, since the increased coronary blood flow secondary to vasodilatation reduces the inflow saturation effects [91, 92]. Figure 17.5 demonstrates impact of sublingual isosorbide dinitrate administration on 3D targeted coronary MRI up to 30 min after drug administration in terms of subjective image quality and objective SNR and vessel sharpness.

The administration of exogenous gadolinium contrast agents (both extracellular [16, 93, 94] and intravascular [95–100]) that shorten the T_1 relaxation time provides an alternative flow-independent approach to improve SNR and CNR. Since conventional extracellular contrast agents, e.g. gadopentetate dimeglumine (Gd-DTPA), diffuse rapidly into

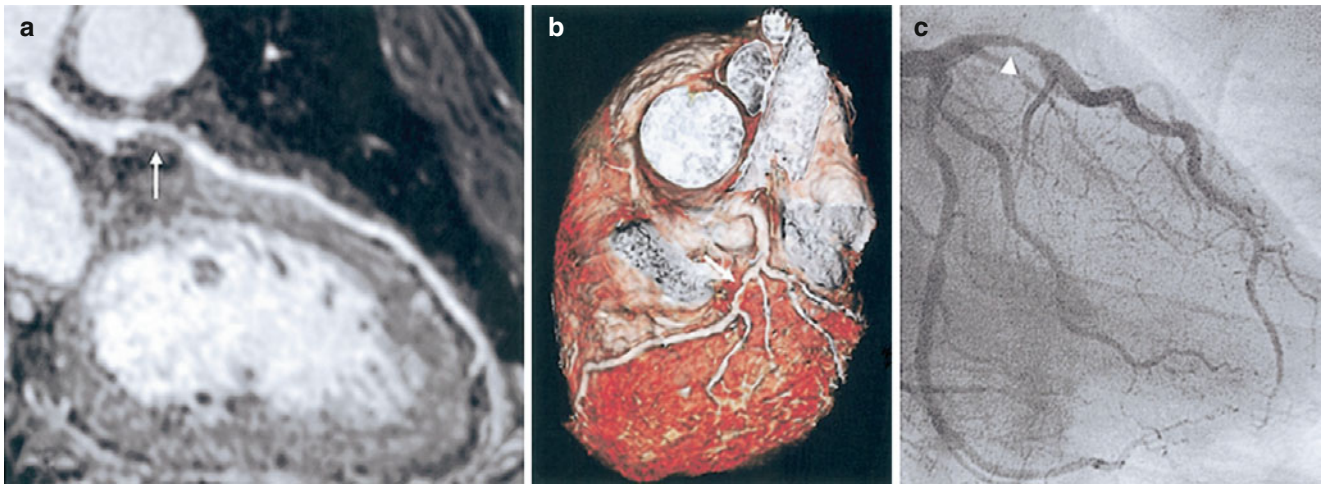

Fig. 17.4 Whole-heart coronary MRI. (**a**) A stenosis in LAD is visualized using a curved multiplanar reconstruction (*white arrow*). (**b**) A three-dimensional view of LAD with stenosis is depicted in the volume-rendered image. (**c**) X-ray coronary angiography confirms proximal LAD stenosis (*arrowhead*) (Adapted from Ref. [26], with permission of Elsevier)

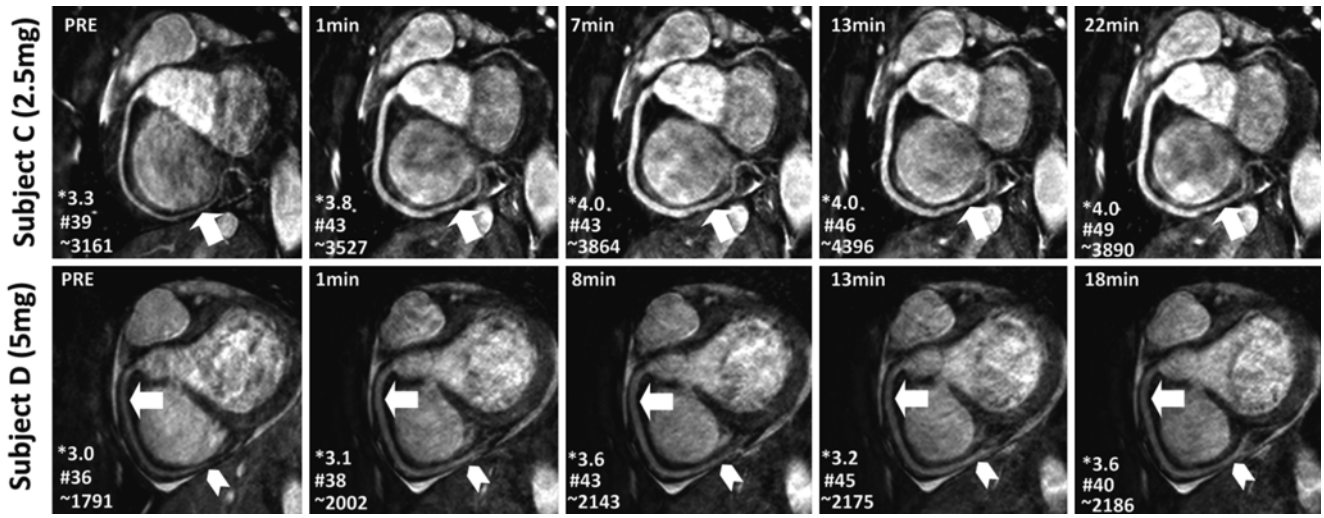

Fig. 17.5 Reformatted images from a targeted 3D coronary MRI of the RCA acquired before and after sublingual isosorbide dinitrate administration on two healthy subjects using a 3D free-breathing SSFP with 2.5 mg (*top row*) and 5 mg doses (*bottom row*) as a function of time. Improved RCA vasodilation and signal enhancement can be observed in all images post-isosorbide dinitrate (*arrows in top* and *bottom row*). The enhanced SNR with isosorbide dinitrate also allows for improved visualization of the distal segments

the interstitial space, early contrast-enhanced coronary MRI studies focused on breath-hold technique to take advantage of the first-passage of these agents [94]. However, both the breath-hold and first-pass aspects of such approaches limit the spatial resolution and is unsuitable for whole-heart coronary acquisitions [29]. Following the availability of a high relaxivity extracellular contrast agent, gadobenate dimeglumine (Gd-BOPTA; MultiHance; Bracco Imaging SpA, Milan, Italy), improved whole-heart coronary MRI at 3 T was shown to be feasible using a T_1-weighted inversion recovery (IR) GRE sequence with a slow infusion of this Gd-BOPTA [16]. An example of contrast-enhanced whole-heart coronary MR image from a CAD patient and the corresponding x-ray angiogram are shown in Fig. 17.6, demonstrating agreement between two modalities in detecting significant stenosis. In a single center trial, 3 T whole-heart coronary MRA with slow infusion of Gd-BOPTA had 93 % sensitivity, 89 % specificity and 90 % accuracy for detecting >50 % diameter stenosis on a per-vessel basis (and 94 %, 82 % and 89 % on a per-patient basis) when compared with x-ray angiography [36]. A bolus infusion of Gd-BOPTA for coronary MRI has also been reported [101], and an example depicted in Fig. 17.7 shows a clear visualization of the three major coronary vessels in the reformatted and 3D volume rendered images. Furthermore, the bolus contrast injection method is advantageous in multiple ways, since it simplifies the initiation time of coronary MRI acquisition compared to slow infusion, and it is compatible with late gadolinium enhancement imaging, which enables the assessment of coronary artery stenosis and myocardium viability using a single bolus contrast injection.

Coronary MRI: Advanced Methods

The sensitivity and specificity of coronary MRI for detection of CAD remain moderate based on single-center [26, 27, 30–34, 36] (Table 17.1) and multi-center [10, 35, 37] studies, despite the tremendous technical improvements in the last two decades. Coronary motion, SNR and CNR remain as major impediments to coronary MRI, and these issues need to be addressed before clinical prime time for coronary MRI. To overcome some of these hurdles, several CMR centers continue with the development and implementation of novel approaches, including non-Cartesian acquisitions, accelerated imaging techniques, coronary vein MRI and higher field imaging.

Non-Cartesian acquisitions provide efficient k-space traversals that lead to incoherent or less visually significant artifacts. Thus, alternative non-Cartesian k-space acquisitions, including spiral and radial coronary MRI have received attention. The use of spiral coronary artery MRI was first reported by Meyer and colleagues [102]. Spiral acquisitions are advantageous to Cartesian acquisitions in several respects, including a more efficient filling of k-space, enhanced SNR [40, 103], and favorable flow properties. However, there are also drawbacks associated with spiral trajectories, such as increased sensitivity to magnetic field inhomogeneity and longer image reconstruction. Interleaved spiral imaging is typically used due to reduced artifacts [102–105], though a single-shot k-space trajectory can also be employed. Both breath-hold (2D) and free-breathing/navigator-gated acquisitions can be performed with spiral coronary imaging [40, 95, 103, 105]. Compared to conventional Cartesian approaches, single spiral acquisitions (per R-R interval) afford a near threefold improvement in SNR [40, 103]. Hence, acquiring two spirals during each R-R interval will halve the acquisition time, while maintaining superior SNR (vs. Cartesian acquisition) and CNR. Variable density spirals have also shown benefit [82].

Radial trajectories also enable more rapid acquisitions, while decreasing sensitivity to motion. Data in healthy subjects appear promising [40, 106–108] and may be particularly beneficial for coronary wall imaging [70, 109, 110].

Parallel imaging techniques such as generalized autocalibrating partially parallel acquisition (GRAPPA) [111] or sensitivity encoding (SENSE) [112] are the most commonly used clinical acceleration technique for coronary MRI [16, 36, 100, 101]. Resultant acceleration rates of up to twofold while using 5–16 element cardiac-coil arrays, and up-to fourfold acceleration rate using 32-channel coils have been achieved [24, 113]. Currently, parallel imaging is considered the state-of-the-art accelerated imaging technique for whole-heart coronary MRI, and is commonly utilized for clinical imaging.

In addition to the non-Cartesian trajectories [114] described previously, compressed sensing (CS) has emerged as an alternative acceleration technique that exploits the sparsity of the image in a transform domain [115, 116]. CS also requires an incoherent undersampling pattern, which can be achieved by random undersampling of k-space data in the k_y-k_z plane for three-dimensional (3D) Cartesian acquisitions. In high-resolution coronary MRI, an advanced CS-based reconstruction strategy was shown to provide reconstructions with reduced blurring compared to conventional CS techniques [117], and was successfully utilized in contrast-enhanced whole-heart coronary MRI [118]. More recently, for highly-accelerated sub-millimeter resolution whole-heart coronary MRI, CS was shown to outperform parallel imaging at sixfold accelerated imaging in a head-to-head comparison [119], with example images depicted in Fig. 17.8. CS can also be used in conjunction with non-Cartesian imaging, such as with spiral acquisitions to enable whole heart acquisitions in a single prolonged breath-hold [81] or with 3D radial trajectories [108].

Coronary MRI at high fields has been an active area of research, due to potential benefits in SNR and CNR. SNR is directly related to field strength (B_0), and thus 3 T imaging

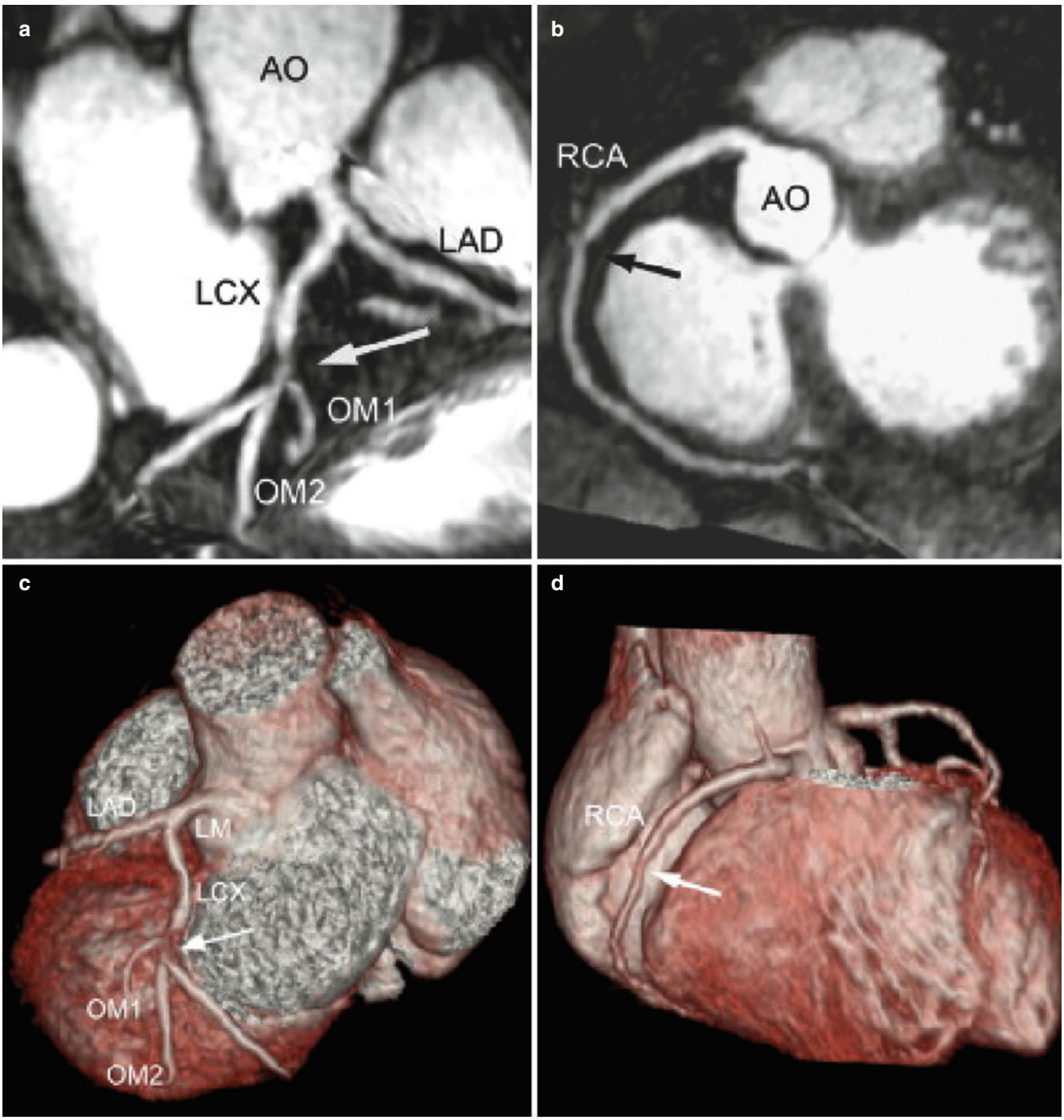

Fig. 17.6 Contrast-enhanced whole-heart 3D coronary MRI with a slow infusion of Gd-BOPTA contrast agent in a patient with atypical chest pain. (**a**, **b**) Contrast-enhanced whole-heart maximum intensity projection images show a significant stenosis in the proximal LCX and a non-significant stenosis in the middle RCA (*arrows*), respectively. (**c**, **d**) The volume-rendered images have the same findings in LCX and RCA (*arrows*). These were consistent with the findings (*arrows*) of conventional coronary angiography (**e**, **f**). *AO* aorta, *OM* obtuse marginal artery (Adapted from Ref. [36], with permission of Elsevier)

would offer the opportunity to double SNR compared to 1.5 T systems [120]. While the vast majority of coronary artery MRI investigations have been performed on 1.5 T systems, clinical 3 T systems are increasingly available and becoming the platform of choice for testing of many advances.

Technical challenges associated with 3 T coronary MRI include increased susceptibility artifacts, field inhomogeneities [87], reduced T_2* [121, 122], increased specific absorption rate (SAR), T_1 prolongation and the amplified magnetohydrodynamic effect [42]. At 3 T, free breathing

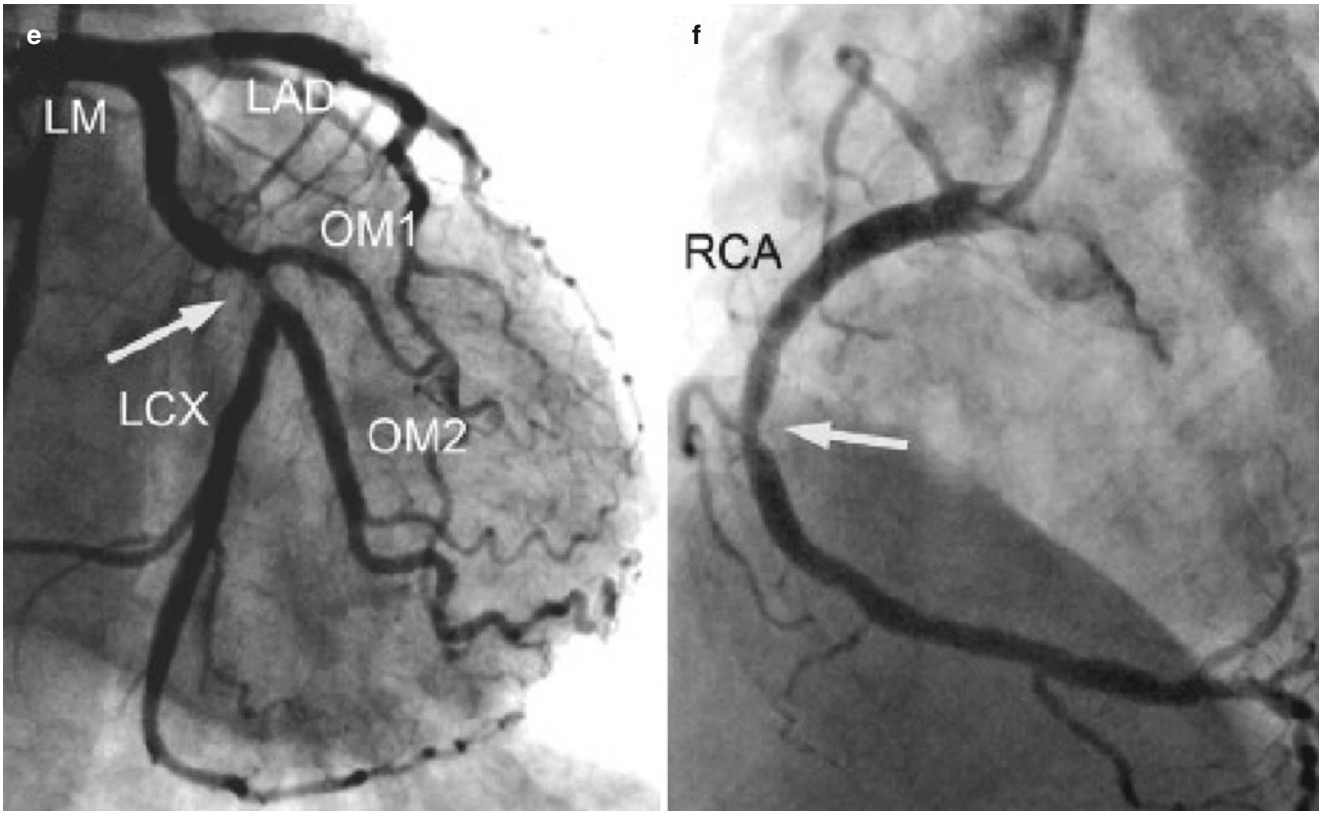

Fig. 17.6 (continued)

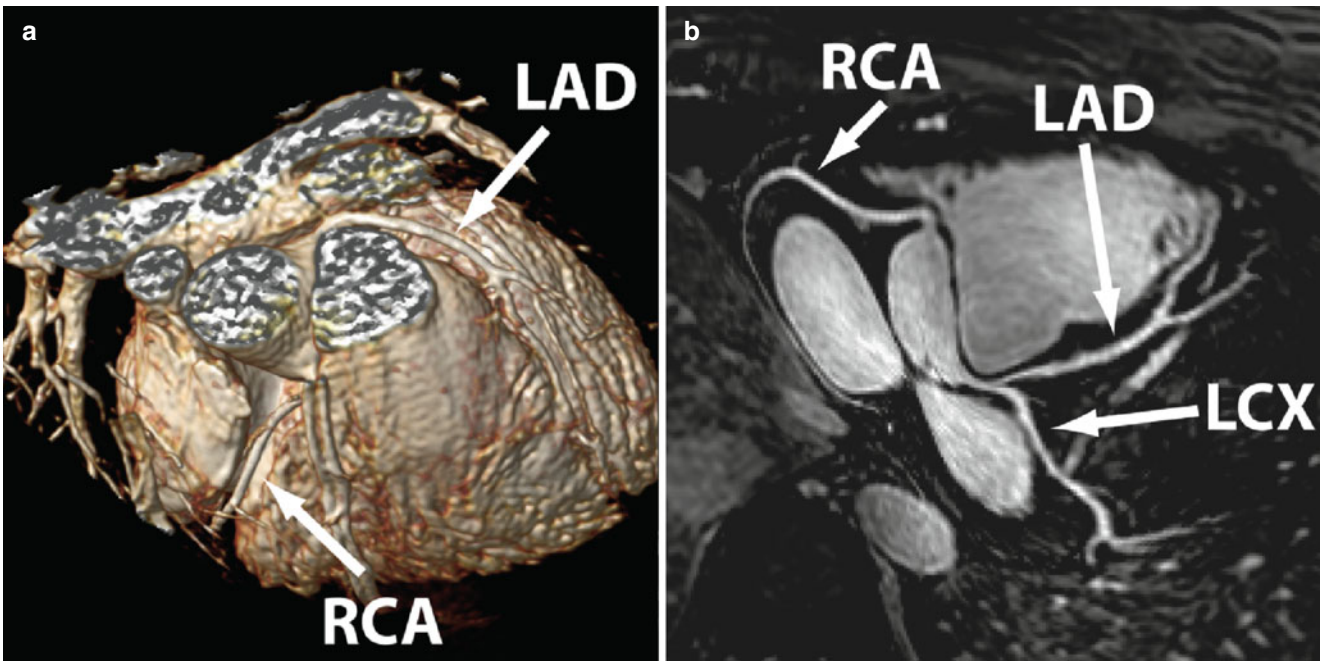

Fig. 17.7 Whole heart SSFP coronary MRI acquired with a bolus injection of Gd-BOPTA. (**a**) 3D volume rendering of the acquisition volume. (**b**) Corresponding reformatted whole-heart image. All three major coronary arteries and distal branches are clearly depicted. *RCA* right coronary artery, *LAD* left anterior descending, *LCX* left circumflex

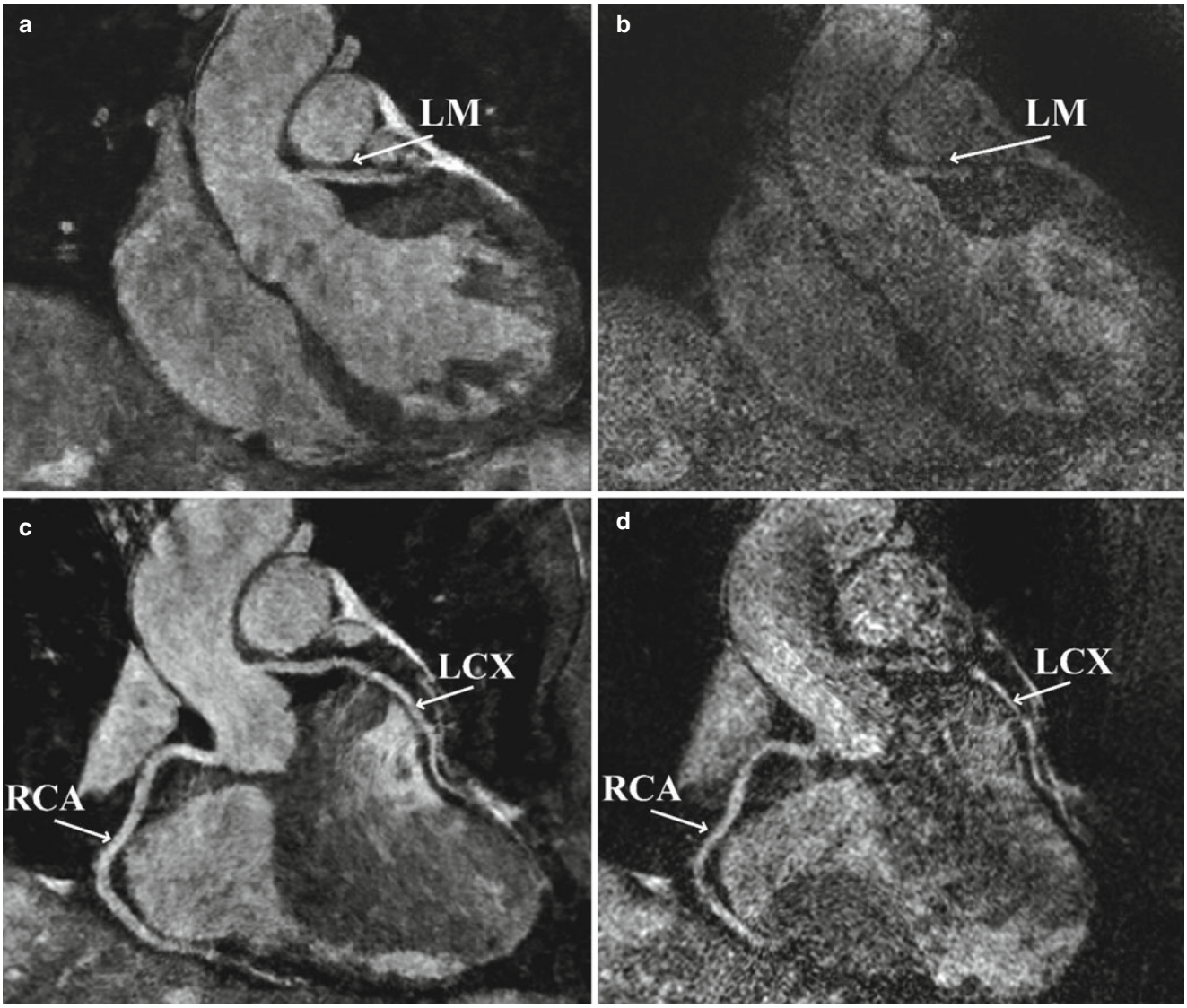

Fig. 17.8 Example images from two separate highly-accelerated sub-millimeter resolution whole-heart coronary MRI. An example coronal slice (*top*) containing a cross-section of the left main (*LM*) shows that SENSE images, acquired with sixfold uniform undersampling (*right*), suffers from noise amplification. In contrast, the LM is clearly visualized using an advanced CS-based technique (LOST), acquired using sixfold random undersampling (*left*). In the reformatted coronal images (*bottom*), the proximal LCX cannot be tracked due to the high noise level in the SENSE reconstruction, but RCA and LCX branches are visualized with the LOST technique

navigator and breath-hold 3D coronary artery MRI studies in healthy volunteers have demonstrated >50 % improvement in SNR with impressive image quality using segmented k-space gradient echo or SSFP [123], as well as spiral and contrast enhanced methods [88, 124, 125]. Coronary MRI at 3 T using SSFP sequences is challenging due to increased field inhomogeneity and high SAR, thus GRE sequences have become widely used for coronary MRI at 3 T. To reduce the impact of B_1 inhomogeneity at the high field strengths, improved preparation sequences such as adiabatic T_2 magnetization preparation [87, 90] and adiabatic fat saturation have also been utilized. Figure 17.9 shows an example of coronary MR images acquired at 3 T using improved T_2 magnetization preparation, which suppresses the banding artifact resulting from conventional T_2 magnetization preparation. Despite these technical improvements, there are currently no multi-center data on a head-to-head comparison between 3 and 1.5 T coronary MRI for diagnosing CAD. Coronary MRI at even higher field strengths, such as 7 T [126], is even more challenging. Figure 17.10 shows an example coronary MRI from a healthy subject acquired at 7 T. Several technical issues, including coil design, motion compensation and B_0 and B_1 field inhomogeneity, need to be addressed before clinical evaluation is possible.

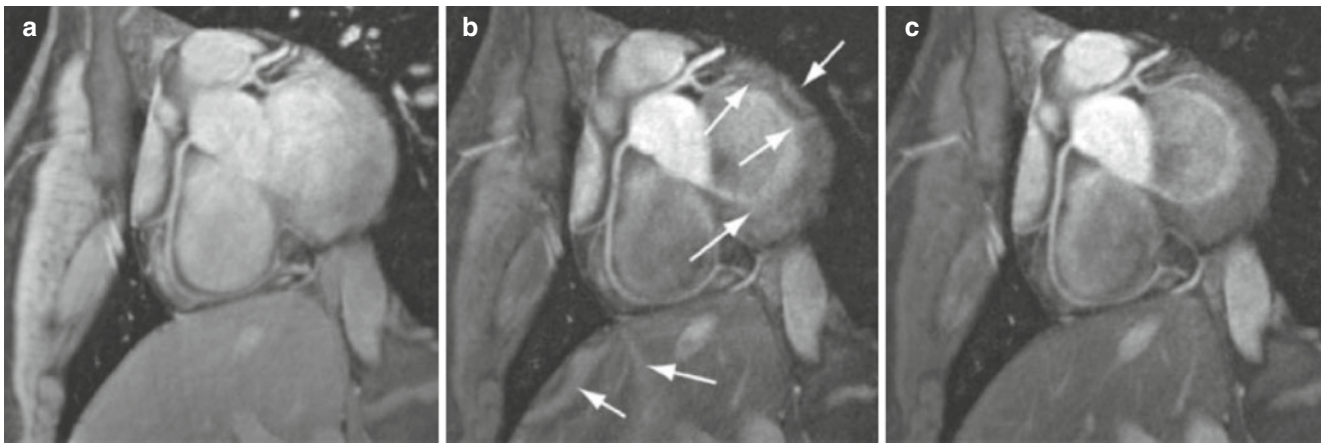

Fig. 17.9 Reformatted 3D coronary MRI of the right coronary artery at 3T (**a**) acquired with no T_2-Prep; (**b**) with T_2-Prep; (**c**) with adiabatic T_2-Prep. *Arrows* in (**b**) point to the artifacts resulting from T_2-Prep sequence. The banding artifacts are suppressed in (**c**), where the homogeneity of the signal is also improved

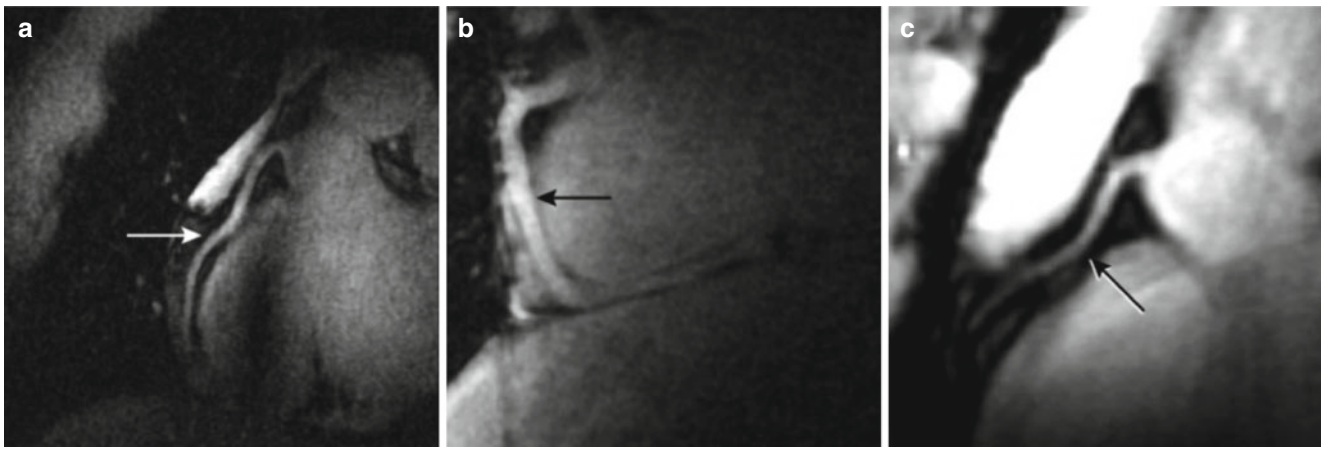

Fig. 17.10 7T coronary MRI of the right coronary artery acquired using a gradient echo imaging sequence. Proximal (**a**, **c**) and more distal (**b**) segments of the RCA are visualized (*arrows*) (Adapted from Ref. [126], with permission of Wiley)

Coronary Vein MRI

For several interventional cardiac procedures, including epicardial radiofrequency ablation [127, 128], retrograde perfusion therapy in high-risk or complicated coronary angioplasty [129], arrhythmia assessment [130, 131], stem cell delivery [132], coronary artery bypass surgery [133] and cardiac resynchronization therapy (CRT) [134, 135], there has been increased interest in imaging the coronary vein anatomy. In CRT, simultaneous pacing of the right ventricle and left ventricle (LV), or pacing the LV alone, results in hemodynamic improvement and restoration of a more physiological contraction pattern [136]. One of the technical difficulties of CRTs is achieving effective, safe and permanent pacing of the LV. Transvenous coronary sinus pacing is the most common technique as it has the least procedural risk, but it is associated with long procedure times, extensive radiation exposure from fluoroscopy, implantation failure and LV lead dislodgment. Two of the major difficulties of the transvenous approach are the small number of coronary vein branches adjacent to an appropriate LV wall and the great variability in coronary vein anatomy [135]. Ideally, coronary venous morphology should be assessed noninvasively prior to CRT procedure, to determine whether epicardial or transvenous lead placement would be more appropriate.

The technical challenges of coronary vein MRI are similar to coronary artery MRI, and techniques developed for coronary artery MRI are widely applicable. Notable differences in coronary vein MRI include the magnetization preparation methods and optimal time window for imaging within the cardiac cycle, as well as more modest spatial resolution requirements since information regarding vein anatomy and vessel size are desired, but not focal stenoses. Magnetization transfer preparation has been utilized in coro-

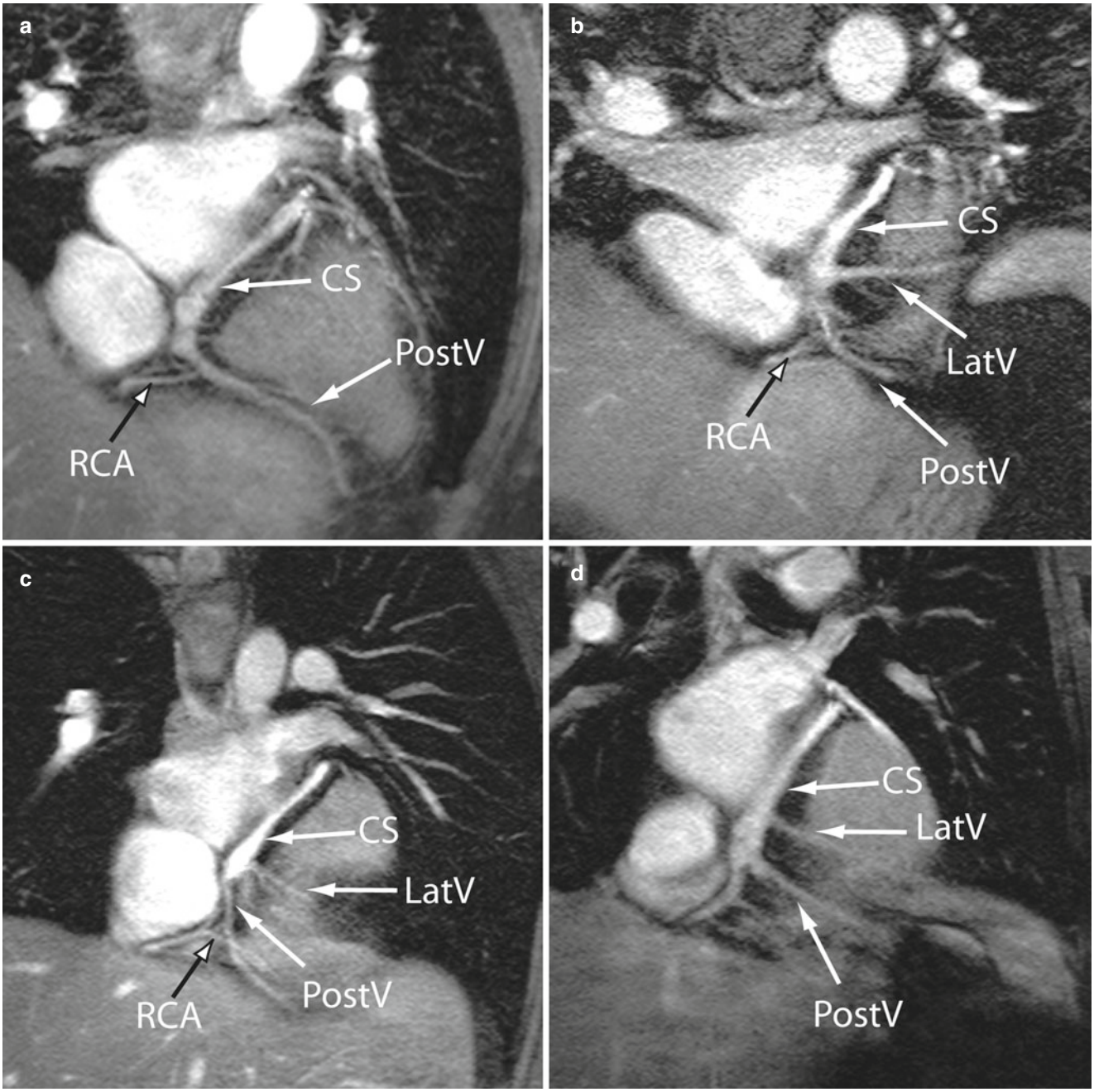

Fig. 17.11 Example coronary vein MRI acquired using magnetization transfer GRE during the systolic rest period, depicting the variations in the coronary venous anatomy in four healthy adult subjects (**a**-**d**). Clear variations in the branching point, angle, and diameter of different tributaries of coronary sinus are observed, highlighting the potential for non-invasive assessment of the coronary venous anatomy in cardiac resynchronization therapy. For example, subject (**a**) has no visible lateral vein (*LatV*)

nary vein imaging, which is different than the T_2 magnetization preparation commonly used in coronary artery MRI, for both targeted [137] and whole-heart [138] approaches. Figure 17.11 shows example coronary vein MRI using a targeted approach with a magnetization transfer preparation sequence. Contrast in coronary vein MRI can be improved by other means, such as the use of intravascular contrast agents such as gadocoletic acid trisodium salt [139] or the use of high relaxivity extracellular contrast agents such as Gd-BOPTA [101]. For the optimal window of imaging, while coronary artery MRI is commonly performed during mid-diastolic quiescent period, coronary vein MRI is acquired in the end-systolic quiescent period as it coincides with the maximum size of the coronary veins [137].

Conclusion

The current clinical applications of coronary artery MRI are limited to evaluation of coronary anomalies and coronary artery aneurysms. For the evaluation of coronary artery stenosis, coronary MRI is able to assess left main and proximal portions of the epicardial coronary arteries. However, due to technical limitations in spatial resolution the evaluation of distal coronary arteries and small side branches is not adequate for routine clinical use. Ongoing technical advances in image acquisition and post-processing have the potential to improve clinical applications of coronary MRI.

References

1. Go AS, et al. Heart disease and stroke statistics – 2013 update: a report from the American Heart Association. Circulation. 2013;127(1):e6–245.
2. Patel MR, et al. Low diagnostic yield of elective coronary angiography. N Engl J Med. 2010;362(10):886–95.
3. Johnson LW, et al. Coronary arteriography 1984–1987, a report of the registry of the society for cardiac angiography and interventions. I. Results and complications. Cathet Cardiovasc Diagn. 1989;17(1):5–10.
4. Davidson CJ, et al. Thrombotic and cardiovascular complications related to nonionic contrast media during cardiac catheterization: analysis of 8,517 patients. Am J Cardiol. 1990;65(22):1481–4.
5. Omran H, et al. Silent and apparent cerebral embolism after retrograde catheterisation of the aortic valve in valvular stenosis: a prospective, randomised study. Lancet. 2003;361(9365):1241–6.
6. Hendel RC, et al. ACCF/ACR/SCCT/SCMR/ASNC/NASCI/SCAI/SIR 2006 appropriateness criteria for cardiac computed tomography and cardiac magnetic resonance imaging: a report of the American College of Cardiology Foundation Quality Strategic Directions Committee Appropriateness Criteria Working Group, American College of Radiology, Society of Cardiovascular Computed Tomography, Society for Cardiovascular Magnetic Resonance, American Society of Nuclear Cardiology, North American Society for Cardiac Imaging, Society for Cardiovascular Angiography and Interventions, and Society of Interventional Radiology. J Am Coll Cardiol. 2006;48(7):1475–97.
7. Hundley WG, et al. ACCF/ACR/AHA/NASCI/SCMR 2010 expert consensus document on cardiovascular magnetic resonance. A report of the American College of Cardiology Foundation Task Force on Expert Consensus Documents. Circulation. 2010;121:2462–508.
8. Manning WJ, Edelman RR. Magnetic resonance coronary angiography. Magn Reson Q. 1993;9(3):131–51.
9. Manning WJ, Li W, Edelman RR. A preliminary report comparing magnetic resonance coronary angiography with conventional angiography. N Engl J Med. 1993;328(12):828.
10. Kim WY, et al. Coronary magnetic resonance angiography for the detection of coronary stenoses. N Engl J Med. 2001;345(26):1863–9.
11. Stuber M, et al. Breathhold three-dimensional coronary magnetic resonance angiography using real-time navigator technology. J Cardiovasc Magn Reson. 1999;1(3):233–8.
12. Stuber M, et al. Submillimeter three-dimensional coronary MR angiography with real-time navigator correction: comparison of navigator locations. Radiology. 1999;212(2):579–87.
13. Stuber M, et al. Double-oblique free-breathing high resolution three-dimensional coronary magnetic resonance angiography. J Am Coll Cardiol. 1999;34(2):524–31.
14. Botnar RM, et al. Improved coronary artery definition with T2-weighted, free-breathing, three-dimensional coronary MRA. Circulation. 1999;99(24):3139–48.
15. Bhat H, et al. Whole-heart contrast-enhanced coronary magnetic resonance angiography using gradient echo interleaved EPI. Magn Reson Med. 2009;61(6):1388–95.
16. Bi X, Carr JC, Li D. Whole-heart coronary magnetic resonance angiography at 3 Tesla in 5 minutes with slow infusion of Gd-BOPTA, a high-relaxivity clinical contrast agent. Magn Reson Med. 2007;58(1):1–7.
17. Bi X, et al. Coronary artery magnetic resonance angiography (MRA): a comparison between the whole-heart and volume-targeted methods using a T2-prepared SSFP sequence. J Cardiovasc Magn Reson. 2006;8(5):703–7.
18. Kim YJ, et al. Feasibility and diagnostic accuracy of whole heart coronary MR angiography using free-breathing 3D balanced turbo-field-echo with SENSE and the half-fourier acquisition technique. Korean J Radiol. 2006;7(4):235–42.
19. Lai P, et al. A respiratory self-gating technique with 3D-translation compensation for free-breathing whole-heart coronary MRA. Magn Reson Med. 2009;62:731–8.
20. Lai P, et al. A dual-projection respiratory self-gating technique for whole-heart coronary MRA. J Magn Reson Imaging. 2008;28(3):612–20.
21. Liu X, et al. Contrast-enhanced whole-heart coronary magnetic resonance angiography at 3.0 T: comparison with steady-state free precession technique at 1.5 T. Invest Radiol. 2008;43(9):663–8.
22. Maintz D, et al. Whole-heart coronary magnetic resonance angiography: value for the detection of coronary artery stenoses in comparison to multislice computed tomography angiography. Acta Radiol. 2007;48(9):967–73.
23. Nehrke K, et al. Free-breathing whole-heart coronary MR angiography on a clinical scanner in four minutes. J Magn Reson Imaging. 2006;23(5):752–6.
24. Niendorf T, et al. Toward single breath-hold whole-heart coverage coronary MRA using highly accelerated parallel imaging with a 32-channel MR system. Magn Reson Med. 2006;56(1):167–76.
25. Okada T, et al. Whole-heart coronary magnetic resonance angiography with parallel imaging: comparison of acceleration in one-dimension vs. two-dimensions. Eur J Radiol. 2009;71(3):486–91.
26. Sakuma H, et al. Detection of coronary artery stenosis with whole-heart coronary magnetic resonance angiography. J Am Coll Cardiol. 2006;48(10):1946–50.
27. Sakuma H, et al. Assessment of coronary arteries with total study time of less than 30 minutes by using whole-heart coronary MR angiography. Radiology. 2005;237(1):316–21.
28. Stehning C, et al. Free-breathing whole-heart coronary MRA with 3D radial SSFP and self-navigated image reconstruction. Magn Reson Med. 2005;54(2):476–80.
29. Weber OM, Martin AJ, Higgins CB. Whole-heart steady-state free precession coronary artery magnetic resonance angiography. Magn Reson Med. 2003;50(6):1223–8.
30. Bunce NH, et al. Evaluation of free-breathing three-dimensional magnetic resonance coronary angiography with hybrid ordered phase encoding (HOPE) for the detection of proximal coronary artery stenosis. J Magn Reson Imaging. 2001;14(6):677–84.
31. Sommer T, et al. Submillimeter 3D coronary MR angiography with real-time navigator correction in 107 patients with suspected coronary artery disease. Röfo. 2002;174(4):459–66.
32. Bogaert J, et al. Coronary artery imaging with real-time navigator three-dimensional turbo-field-echo MR coronary angiography: initial experience. Radiology. 2003;226(3):707–16.
33. Jahnke C, et al. Coronary MR angiography with steady-state free precession: individually adapted breath-hold technique versus free-breathing technique. Radiology. 2004;232(3):669–76.
34. Pouleur AC, et al. Direct comparison of whole-heart navigator-gated magnetic resonance coronary angiography and 40- and 64-slice multidetector row computed tomography to detect the coronary artery stenosis in patients scheduled for conventional coronary angiography. Circ Cardiovasc Imaging. 2008;1(2):114–21.

35. Kato S, et al. Assessment of coronary artery disease using magnetic resonance coronary angiography: a national multicenter trial. J Am Coll Cardiol. 2010;56(12):983–91.
36. Yang Q, et al. Contrast-enhanced whole-heart coronary magnetic resonance angiography at 3.0-T: a comparative study with X-ray angiography in a single center. J Am Coll Cardiol. 2009;54(1): 69–76.
37. Yang Q, et al. Assessment of coronary artery disease using 3.0 T magnetic resonance coronary angiography: a national multicenter trial. J Cardiovasc Magn Reson. 2013;15 Suppl 1:E5.
38. Deshpande VS, et al. 3D magnetization-prepared true-FISP: a new technique for imaging coronary arteries. Magn Reson Med. 2001;46(3):494–502.
39. Nezafat R, et al. Inflow quantification in three-dimensional cardiovascular MR imaging. J Magn Reson Imaging. 2008;28(5):1273–9.
40. Maintz D, et al. Coronary MR angiography: comparison of quantitative and qualitative data from four techniques. AJR Am J Roentgenol. 2004;182(2):515–21.
41. Ozgun M, et al. Comparison of 3D segmented gradient-echo and steady-state free precession coronary MRI sequences in patients with coronary artery disease. AJR Am J Roentgenol. 2005; 185(1):103–9.
42. Polson MJ, Barker AT, Gardiner S. The effect of rapid rise-time magnetic fields on the ECG of the rat. Clin Phys Physiol Meas. 1982;3(3):231–4.
43. Paulin S. Coronary angiography. A technical, anatomic and clinical study. Acta Radiol Diagn. 1964;54(Suppl 233):L+.
44. Wang Y, Vidan E, Bergman GW. Cardiac motion of coronary arteries: variability in the rest period and implications for coronary MR angiography. Radiology. 1999;213(3):751–8.
45. Kaji S, et al. Rapid evaluation of left ventricular volume and mass without breath-holding using real-time interactive cardiac magnetic resonance imaging system. J Am Coll Cardiol. 2001;38(2):527–33.
46. Hofman MB, Wickline SA, Lorenz CH. Quantification of in-plane motion of the coronary arteries during the cardiac cycle: implications for acquisition window duration for MR flow quantification. J Magn Reson Imaging. 1998;8(3):568–76.
47. Kim WY, et al. Impact of bulk cardiac motion on right coronary MR angiography and vessel wall imaging. J Magn Reson Imaging. 2001;14(4):383–90.
48. Jahnke C, et al. A new approach for rapid assessment of the cardiac rest period for coronary MRA. J Cardiovasc Magn Reson. 2005;7(2):395–9.
49. Leiner T, et al. Correction for heart rate variability improves coronary magnetic resonance angiography. J Magn Reson Imaging. 2005;22(4):577–82.
50. Jahnke C, Paetsch I, Gebker R, Schnackenburg B, Bornstedt A, Fleck E, et al. Comparison of individually adapted breath-hold and free-breathing coronary MRA using steady state free precession [abstr]. J Cardiovasc Magn Reson. 2004;6:166–7.
51. Plein S, et al. Three-dimensional coronary MR angiography performed with subject-specific cardiac acquisition windows and motion-adapted respiratory gating. AJR Am J Roentgenol. 2003;180(2):505–12.
52. Tangcharoen T, et al. Impact of heart rate variability in patients with normal sinus rhythm on image quality in coronary magnetic angiography. J Magn Reson Imaging. 2008;28(1):74–9.
53. Wang Y, Riederer SJ, Ehman RL. Respiratory motion of the heart: kinematics and the implications for the spatial resolution in coronary imaging. Magn Reson Med. 1995;33(5):713–9.
54. Edelman RR, et al. Coronary arteries: breath-hold MR angiography. Radiology. 1991;181(3):641–3.
55. Taylor AM, et al. MR navigator-echo monitoring of temporal changes in diaphragm position: implications for MR coronary angiography. J Magn Reson Imaging. 1997;7(4):629–36.
56. Holland AE, Goldfarb JW, Edelman RR. Diaphragmatic and cardiac motion during suspended breathing: preliminary experience and implications for breath-hold MR imaging. Radiology. 1998;209(2):483–9.
57. Danias PG, et al. Navigator assessment of breath-hold duration: impact of supplemental oxygen and hyperventilation. AJR Am J Roentgenol. 1998;171(2):395–7.
58. Ehman RL, Felmlee JP. Adaptive technique for high-definition MR imaging of moving structures. Radiology. 1989;173(1): 255–63.
59. Oshinski JN, et al. Two-dimensional coronary MR angiography without breath holding. Radiology. 1996;201(3):737–43.
60. Sachs TS, et al. Real-time motion detection in spiral MRI using navigators. Magn Reson Med. 1994;32(5):639–45.
61. McConnell MV, et al. Comparison of respiratory suppression methods and navigator locations for MR coronary angiography. AJR Am J Roentgenol. 1997;168(5):1369–75.
62. Danias PG, et al. Prospective navigator correction of image position for coronary MR angiography. Radiology. 1997;203(3):733–6.
63. McConnell MV, et al. Prospective adaptive navigator correction for breath-hold MR coronary angiography. Magn Reson Med. 1997;37(1):148–52.
64. Moghari MH, et al. Subject-specific estimation of respiratory navigator tracking factor for free-breathing cardiovascular MR. Magn Reson Med. 2012;67(6):1665–72.
65. McConnell M, et al. Comparison of respiratory suppression methods and navigator locations for MR coronary angiography. Am J Roentgenol. 1997;168(5):1369.
66. Nezafat R, et al. Improved spatial-temporal resolution MR coronary blood flow imaging at 3T. J Cardiovasc Magn Reson. 2005;7(1):199.
67. Nehrke K, Bornert P. Prospective correction of affine motion for arbitrary MR sequences on a clinical scanner. Magn Reson Med. 2005;54(5):1130–8.
68. Lai P, et al. Respiratory self-gated four-dimensional coronary MR angiography: a feasibility study. Magn Reson Med. 2008;59(6): 1378–85.
69. Larson AC, et al. Preliminary investigation of respiratory self-gating for free-breathing segmented cine MRI. Magn Reson Med. 2005;53(1):159–68.
70. Park J, et al. 4D radial coronary artery imaging within a single breath-hold: cine angiography with phase-sensitive fat suppression (CAPS). Magn Reson Med. 2005;54(4):833–40.
71. Keegan J, et al. Non-model based correction of respiratory motion using beat-to-beat 3D spiral fat-selective imaging. J Magn Reson Imaging. 2007;26(3):624–9.
72. Nguyen T, et al. Free-breathing 3D steady-state free precession coronary magnetic resonance angiography: Comparison of diaphragm and cardiac fat navigators. J Magn Reson Imaging: JMRI. 2008;28(2):509.
73. Nguyen T, et al. 2128 Free-breathing steady-state free precession 3D coronary MRA: comparison of diaphragm and cardiac fat navigator techniques. J Cardiovasc Magn Reson. 2008;10 Suppl 1: A397.
74. Nguyen T, et al. Free-breathing 3-dimensional steady-state free precession coronary magnetic resonance angiography: comparison of four navigator gating techniques. Magn Reson Imaging. 2009;27(6):807–14.
75. Uribe S, et al. Whole-heart cine MRI using real-time respiratory self-gating. Magn Reson Med. 2007;57:606–13.
76. Brau AC, Brittain JH. Generalized self-navigated motion detection technique: preliminary investigation in abdominal imaging. Magn Reson Med. 2006;55(2):263–70.
77. Danias PG, et al. Relationship between motion of coronary arteries and diaphragm during free breathing: lessons from real-time MR imaging. AJR Am J Roentgenol. 1999;172(4):1061–5.

78. Nehrke K, et al. Free-breathing cardiac MR imaging: study of implications of respiratory motion – initial results. Radiology. 2001;220(3):810–5.
79. Moghari MH, et al. Free-breathing cardiac MR with a fixed navigator efficiency using adaptive gating window size. Magn Reson Med. 2012;68(6):1866–75.
80. Gurney PT, Hargreaves BA, Nishimura DG. Design and analysis of a practical 3D cones trajectory. Magn Reson Med. 2006;55(3): 575–82.
81. Santos JM, et al. Single breath-hold whole-heart MRA using variable-density spirals at 3T. Magn Reson Med. 2006;55(2): 371–9.
82. Sussman M, et al. Variable-density adaptive imaging for high-resolution coronary artery MRI. Magn Reson Med. 2002;48(5): 753–64.
83. Li D, et al. Coronary arteries: three-dimensional MR imaging with fat saturation and magnetization transfer contrast. Radiology. 1993;187(2):401–6.
84. Brittain JH, et al. Coronary angiography with magnetization-prepared T2 contrast. Magn Reson Med. 1995;33(5):689–96.
85. Shea SM, et al. Three-dimensional true-FISP imaging of the coronary arteries: improved contrast with T2-preparation. J Magn Reson Imaging. 2002;15(5):597–602.
86. Balaban RS, Ceckler TL. Magnetization transfer contrast in magnetic resonance imaging. Magn Reson Q. 1992;8(2):116–37.
87. Nezafat R, et al. B1-insensitive T2 preparation for improved coronary magnetic resonance angiography at 3 T. Magn Reson Med. 2006;55(4):858–64.
88. Stuber M, et al. Preliminary report on in vivo coronary MRA at 3 Tesla in humans. Magn Reson Med. 2002;48(3):425–9.
89. Schar M, Kozerke S, Fischer SE, Boesiger P. Cardiac SSFP imaging at 3 Tesla. Magn Reson Med. 2004;51(4):799–806.
90. Nezafat R, et al. Spectrally selective B1-insensitive T2 magnetization preparation sequence. Magn Reson Med. 2009;61(6): 1326–35.
91. Terashima M, et al. Noninvasive assessment of coronary vasodilation using magnetic resonance angiography. J Am Coll Cardiol. 2005;45(1):104–10.
92. Hu P, et al. Coronary MR imaging: effect of timing and dose of isosorbide dinitrate administration. Radiology. 2010;254(2): 401–9.
93. Zheng J, et al. Efficacy of slow infusion of gadolinium contrast agent in three-dimensional MR coronary artery imaging. J Magn Reson Imaging. 1999;10(5):800–5.
94. Goldfarb JW, Edelman RR. Coronary arteries: breath-hold, gadolinium-enhanced, three-dimensional MR angiography. Radiology. 1998;206(3):830–4.
95. Knuesel PR, et al. Multislice breath-hold spiral magnetic resonance coronary angiography in patients with coronary artery disease: effect of intravascular contrast medium. J Magn Reson Imaging. 2002;16(6):660–7.
96. Herborn CU, et al. Coronary arteries: contrast-enhanced MR imaging with SH L 643A – experience in 12 volunteers. Radiology. 2003;229(1):217–23.
97. Prompona M, et al. Contrast-enhanced whole-heart MR coronary angiography at 3.0T using the intravascular contrast agent gadofosveset. Invest Radiol. 2009;44(7):369–74.
98. Kelle S, et al. Whole-heart coronary magnetic resonance angiography with MS-325 (Gadofosveset). Med Sci Monit. 2007; 13(11):CR469–74.
99. de Haen C, et al. Gadocoletic acid trisodium salt (b22956/1): a new blood pool magnetic resonance contrast agent with application in coronary angiography. Invest Radiol. 2006;41(3):279–91.
100. Tang L, et al. Volume-targeted and whole-heart coronary magnetic resonance angiography using an intravascular contrast agent. J Magn Reson Imaging. 2009;30(5):1191–6.
101. Hu P, et al. Contrast-enhanced whole-heart coronary MRI with bolus infusion of gadobenate dimeglumine at 1.5 T. Magn Reson Med. 2011;65(2):392–8.
102. Meyer CH, et al. Fast spiral coronary artery imaging. Magn Reson Med. 1992;28(2):202–13.
103. Bornert P, et al. Direct comparison of 3D spiral vs. Cartesian gradient-echo coronary magnetic resonance angiography. Magn Reson Med. 2001;46(4):789–94.
104. Thedens DR, et al. Fast magnetic resonance coronary angiography with a three-dimensional stack of spirals trajectory. Magn Reson Med. 1999;41(6):1170–9.
105. Bornert P, Aldefeld B, Nehrke K. Improved 3D spiral imaging for coronary MR angiography. Magn Reson Med. 2001;45(1): 172–5.
106. Leiner T, Yeh E, Katsimaglis G, Kissinger KV, Spuentrup E, Manning WJ, et al. Comparison of cartesian and radial balanced GTFE coronary MRA [abstr]. J Cardiovasc Magn Reson. 2004; 6:75.
107. Weber OM, et al. Free-breathing, three-dimensional coronary artery magnetic resonance angiography: comparison of sequences. J Magn Reson Imaging. 2004;20(3):395–402.
108. Nam S, et al. Compressed sensing reconstruction for whole heart imaging with 3D radial trajectories: a GPU implementation. Magn Reson Med. 2013;69(1):91–102.
109. Botnar RM, et al. Noninvasive coronary vessel wall and plaque imaging with magnetic resonance imaging. Circulation. 2000;102(21):2582–7.
110. Katoh M, et al. MR coronary vessel wall imaging: comparison between radial and spiral k-space sampling. J Magn Reson Imaging. 2006;23(5):757–62.
111. Griswold MA, et al. Generalized autocalibrating partially parallel acquisitions (GRAPPA). Magn Reson Med. 2002;47(6):1202–10.
112. Pruessmann KP, et al. Advances in sensitivity encoding with arbitrary k-space trajectories. Magn Reson Med. 2001;46(4): 638–51.
113. Nagata M, et al. Diagnostic accuracy of 1.5-T unenhanced whole-heart coronary MR angiography performed with 32-channel cardiac coils: initial single-center experience. Radiology. 2011;259(2):384–92.
114. Bhat H, et al. Contrast-enhanced whole-heart coronary magnetic resonance angiography at 3T with radial EPI. Magn Reson Med. 2011;66(1):82–91.
115. Block KT, Uecker M, Frahm J. Undersampled radial MRI with multiple coils. Iterative image reconstruction using a total variation constraint. Magn Reson Med. 2007;57(6):1086–98.
116. Lustig M, Donoho DL, Pauly JM. Sparse MRI: the application of compressed sensing for rapid MR imaging. Magn Reson Med. 2007;58(6):1182–95.
117. Akcakaya M, et al. Low-dimensional-structure self-learning and thresholding: regularization beyond compressed sensing for MRI reconstruction. Magn Reson Med. 2011;66(3):756–67.
118. Akcakaya M, et al. Accelerated contrast-enhanced whole-heart coronary MRI using low-dimensional-structure self-learning and thresholding. Magn Reson Med. 2012;67(5):1434–43.
119. Akcakaya M, et al. Accelerated isotropic sub-millimeter whole-heart coronary MRI: compressed sensing versus parallel imaging. Magn Reson Med. 2014;71(2):815–22.
120. Wen H, et al. The intrinsic signal-to-noise ratio in human cardiac imaging at 1.5, 3, and 4T. J Magn Reson. 1997;125(1):65–71.
121. Noeske R, et al. Human cardiac imaging at 3 T using phased array coils. Magn Reson Med. 2000;44(6):978–82.
122. Atalay MK, et al. Cardiac susceptibility artifacts arising from the heart-lung interface. Magn Reson Med. 2001;45(2):341–5.
123. Bi X, et al. Three-dimensional breathhold SSFP coronary MRA: a comparison between 1.5T and 3.0T. J Magn Reson Imaging. 2005;22(2):206–12.

124. Steen HLJ, Giannitsis E, Katus HA, Stuber M. Comparison of high field magnetic resonance imaging at 1.5T and 3T for coronary artery MRA [abstr]. J Cardiovasc Magn Reson. 2004;6:342–4.
125. Bi X, Deshpande V, Simonetti O, Laub G, Li D. Three-dimensional breath-hold coronary MRA: a comparison between 1.5T and 3.0T [abstr]. J Cardiovasc Magn Reson. 2004;6:335–6.
126. van Elderen SG, et al. Initial results on in vivo human coronary MR angiography at 7 T. Magn Reson Med. 2009;62(6): 1379–84.
127. Kusano KF, et al. Catheter ablation of an epicardial accessory pathway via the middle cardiac vein guided by monophasic action potential recordings. Europace. 2001;3(2):164–7.
128. Haissaguerre M, et al. Radiofrequency catheter ablation of left lateral accessory pathways via the coronary sinus. Circulation. 1992;86(5):1464–8.
129. Kar S, Nordlander R. Coronary veins: an alternate route to ischemic myocardium. Heart Lung. 1992;21(2):148–57.
130. Stellbrink C, et al. Transcoronary venous radiofrequency catheter ablation of ventricular tachycardia. J Cardiovasc Electrophysiol. 1997;8(8):916–21.
131. Butter C, et al. Human experience with transvenous biventricular defibrillation using an electrode in a left ventricular vein. Pacing Clin Electrophysiol. 2002;25(3):324–31.
132. Thompson CA, et al. Percutaneous transvenous cellular cardiomyoplasty. A novel nonsurgical approach for myocardial cell transplantation. J Am Coll Cardiol. 2003;41(11):1964–71.
133. Oesterle SN, et al. Percutaneous in situ coronary venous arterialization: report of the first human catheter-based coronary artery bypass. Circulation. 2001;103(21):2539–43.
134. de Paola AA, et al. Angiographic and electrophysiological substrates for ventricular tachycardia mapping through the coronary veins 1. Heart. 1998;79(1):59–63.
135. Singh JP, et al. The coronary venous anatomy: a segmental approach to aid cardiac resynchronization therapy. J Am Coll Cardiol. 2005;46(1):68–74.
136. Abraham WT, et al. Cardiac resynchronization in chronic heart failure. N Engl J Med. 2002;346(24):1845–53.
137. Nezafat R, et al. Coronary magnetic resonance vein imaging: imaging contrast, sequence, and timing. Magn Reson Med. 2007;58(6):1196–206.
138. Stoeck CT, et al. Whole heart magnetization-prepared steady-state free precession coronary vein MRI. J Magn Reson Imaging. 2009;29(6):1293–9.
139. Rasche V, et al. Whole-heart coronary vein imaging: a comparison between non-contrast-agent-and contrast-agent-enhanced visualization of the coronary venous system. Magn Reson Med. 2007;57(6):1019–26.